

# Geophysical Research Letters

## RESEARCH LETTER

10.1029/2019GL083913

### Key Points:

- Develop a new automatic method to detect dynamic triggering and evaluate its confidence level
- Influence of noise and variations in the background seismicity can be suppressed
- Effectiveness of the new method is demonstrated by applying to the Geysers Geothermal Field

### Supporting Information:

- Supporting Information S1
- Table S1
- Table S2

### Correspondence to:

S. Zhou and H. Yang,  
zsy@pku.edu.cn;  
hyang@cuhk.edu.hk

### Citation:

Yun, N., Zhou, S., Yang, H., Yue, H., & Zhao, L. (2019). Automated detection of dynamic earthquake triggering by the high-frequency power integral ratio. *Geophysical Research Letters*, 46. <https://doi.org/10.1029/2019GL083913>

Received 29 MAY 2019

Accepted 1 OCT 2019

Accepted article online 25 OCT 2019

## Automated Detection of Dynamic Earthquake Triggering by the High-Frequency Power Integral Ratio

Naidan Yun<sup>1</sup>, Shiyong Zhou<sup>1</sup>, Hongfeng Yang<sup>2</sup>, Han Yue<sup>1</sup>, and Li Zhao<sup>1</sup>

<sup>1</sup>School of Earth and Space Sciences, Peking University, Beijing, China, <sup>2</sup>Earth System Science Programme, Faculty of Science, The Chinese University of Hong Kong, Hong Kong, China

**Abstract** Dynamic earthquake triggering can be used to investigate the responses of faults to stress disturbances. We develop a new method to detect dynamic triggering by estimating high-frequency energy change before and during teleseismic waves using the HiFi method. Our method is able to identify local events independent of earthquake catalog or subjective judgements. The significance in energy change is evaluated by a statistical analysis of the background ratio in a large number of days, which can suppress the influence of noise and variations in the background seismicity and yield a confidence level of dynamic triggering (0–1). We apply the HiFi method to the Geysers Geothermal Field in California, and the results are largely consistent with previous reports from the  $\beta$  statistic. By comparing the results of HiFi and  $\beta$  statistic, we select a confidence level range of 0.918–0.947 as the optimum threshold to identify dynamic triggering in the region.

**Plain Language Summary** Dynamic triggering is related to dynamic stress change caused by the passage of teleseismic waves and represents one of the earthquake interactions critical to advancing our understanding of earthquake physics. It can be used to investigate the responses of faults to the stress disturbance so as to monitor the temporal variation in stress status. However, the physical processes of earthquake triggering are still in debate, which require systematic analysis of large amounts of data. Widely used methods to detect dynamic triggering are often time-consuming and depend on local earthquake catalogs or subjective judgements for event identification. We develop a new automatic method to detect dynamic triggering by directly comparing the high-frequency energies before and during the teleseismic waves. Moreover, we suppress the influence of noise and variations in the background seismicity and provide confidence levels for dynamic triggering. We apply our method to the Geysers Geothermal Field, and a comparison with previous results demonstrates its effectiveness.

## 1. Introduction

Large earthquakes can excite seismicity thousands of kilometers away through dynamic triggering, which has been reported by a large number of observations globally (e.g., Anderson et al., 1994; Brodsky & Prejean, 2005; Gomberg et al., 2004; Gomberg & Johnson, 2005; Hill et al., 1993; Johnston et al., 2004; Z. Peng et al., 2009; Y. Peng et al., 2012; Van der Elst et al., 2013; Velasco et al., 2008; Wang et al., 2015). As we can calculate dynamic stresses caused by the teleseismic waves, dynamic triggering can be used to investigate the responses of faults to stress disturbances (Brodsky & van der Elst, 2014; Hill & Prejean, 2007).

Traditional methods for detecting dynamic triggering generally consist of two steps. First, one needs to acquire local earthquake catalogs (Gomberg et al., 2001; Prejean et al., 2004) or manually identify local earthquakes from seismograms before and during the passage of teleseismic waves (Jiang et al., 2010; Z. Peng et al., 2010; Wu et al., 2011). However, manual detection is time-consuming and significantly limits investigations of dynamic triggering over a long time span and/or in a large area. Automatic methods to detect microearthquakes can be applied in this step (Linville et al., 2014; Velasco et al., 2016; Wang et al., 2015), for example, the matched filter technique (Gibbons & Ringdal, 2006; Z. Peng & Zhao, 2009; Yang et al., 2009). However, earthquake templates with even distribution in the research area are important for the matched filter technique, which may be hard to obtain in low seismicity areas. Miyazawa and Mori (2005) replaced the number of earthquakes with the envelop amplitudes of band-pass-filtered seismograms, but the results were greatly affected by near-surface noise. They used seismic records from borehole stations

©2019. The Authors.

This is an open access article under the terms of the Creative Commons Attribution-NonCommercial-NoDerivs License, which permits use and distribution in any medium, provided the original work is properly cited, the use is non-commercial and no modifications or adaptations are made.

with much lower noise levels, which may not be applicable for nonborehole stations. In the second step, the significance of seismicity changes caused by teleseismic waves is evaluated mostly by the  $\beta$  statistic, which estimates the differences between the observed number of local earthquakes during the passage of teleseismic waves and the expected number based on the average seismicity before the teleseismic arrival (e.g., Matthews & Reasenberg, 1988; Reasenberg & Simpson, 1992). Because the null hypothesis of  $\beta$  statistic means no difference in seismicity between the two time windows, it does not differentiate the change in background seismicity, which can be caused by other processes such as earth tides (Cochran et al., 2004). Thus, the accuracy of dynamic triggering determination may be influenced.

We develop a new method to detect dynamic triggering by directly comparing the high-frequency energy before and during the passing teleseismic waves using the High-Frequency power Integral ratio (HiFi). Thus, it does not depend on the earthquake catalog or subjective criteria for event detection and is applicable to large amounts of data. Moreover, we suppress the noise interference and take into account the variation in background seismicity using statistics. Finally, a confidence level (0–1) to evaluate the probability of dynamic triggering can be provided. We apply the HiFi method to the Geysers Geothermal Field in California (supporting information Figure S1), compare the results with those from  $\beta$  statistic test (Aiken & Peng, 2014), and determine the optimal threshold of confidence level for the Geysers area which may be related to the state of regional stress field of the study area and the characteristics of responses to dynamic stress.

## 2. The HiFi Method

### 2.1. Quantifying the Change in High-Frequency Energy

Taking the 2010  $M7.2$  Baja California earthquake as an example, the high-frequency energy is visible in the spectrogram recorded at Station GDXB in the Geysers area (Figure 1a). After filtering the seismogram to  $>25$  Hz, emerged local earthquakes (Figure 1c) coincide with the teleseismic surface waves (Figure 1b) and are indicative of prominent dynamic triggering. By comparing the high-frequency energy before and during the teleseismic waves, we are able to distinguish these triggered local earthquakes automatically.

In order to quantify the energy difference, we calculate the power spectral densities (PSDs) of the seismogram within two time windows:  $T_b$  before the teleseismic arrival and  $T_e$  during the teleseismic waves. The PSD in the  $T_b$  window,  $PSD_b$ , represents background activities, so it should be sufficiently long, for example, several hours to a few days (e.g., Pankow et al., 2004). The PSD in the  $T_e$  window,  $PSD_e$ , may contain signals of triggered earthquakes; thus, its length depends on the triggering potential of waves and is generally much shorter than  $T_b$ . For the 2010 Baja California earthquake (Figure 1b), we select the  $T_e$  to be between the arrival times of waves with speeds of 5 and 2 km/s ( $\sim 300$  s) and the  $T_b$  to be 5 hr. We then calculate the high-frequency energy in each time window by integrating the PSD in the frequency range ( $f_l, f_h$ ; Figure 1d):

$$I_b = \int_{f_l}^{f_h} PSD_b df, \quad (1)$$

$$I_e = \int_{f_l}^{f_h} PSD_e df, \quad (2)$$

where  $I_b$  and  $I_e$  are the integrals of the PSDs in the  $T_b$  and  $T_e$  windows, respectively. The lower-limit  $f_l$  should be high enough to avoid contaminations from the teleseismic waves. Here we choose the frequency range of 25–35 Hz, which will be discussed later in section 3.2.

Next we calculate the logarithmic ratio between  $I_e$  and  $I_b$ :

$$R_E = \log_{10} \frac{I_e}{I_b}. \quad (3)$$

For the 2010 Baja California earthquake that dynamically triggered events in the Geysers area, the logarithmic ratio is 3.96 (Figure 1d). In comparison, the logarithmic ratio is  $-0.83$  for the 2009  $M5.8$  Gulf of California earthquake (Figure 1h). A logarithmic ratio  $<0$  indicates no dynamic triggering, which can be confirmed in the spectrogram and high-pass-filtered seismogram (Figures 1e and 1g).

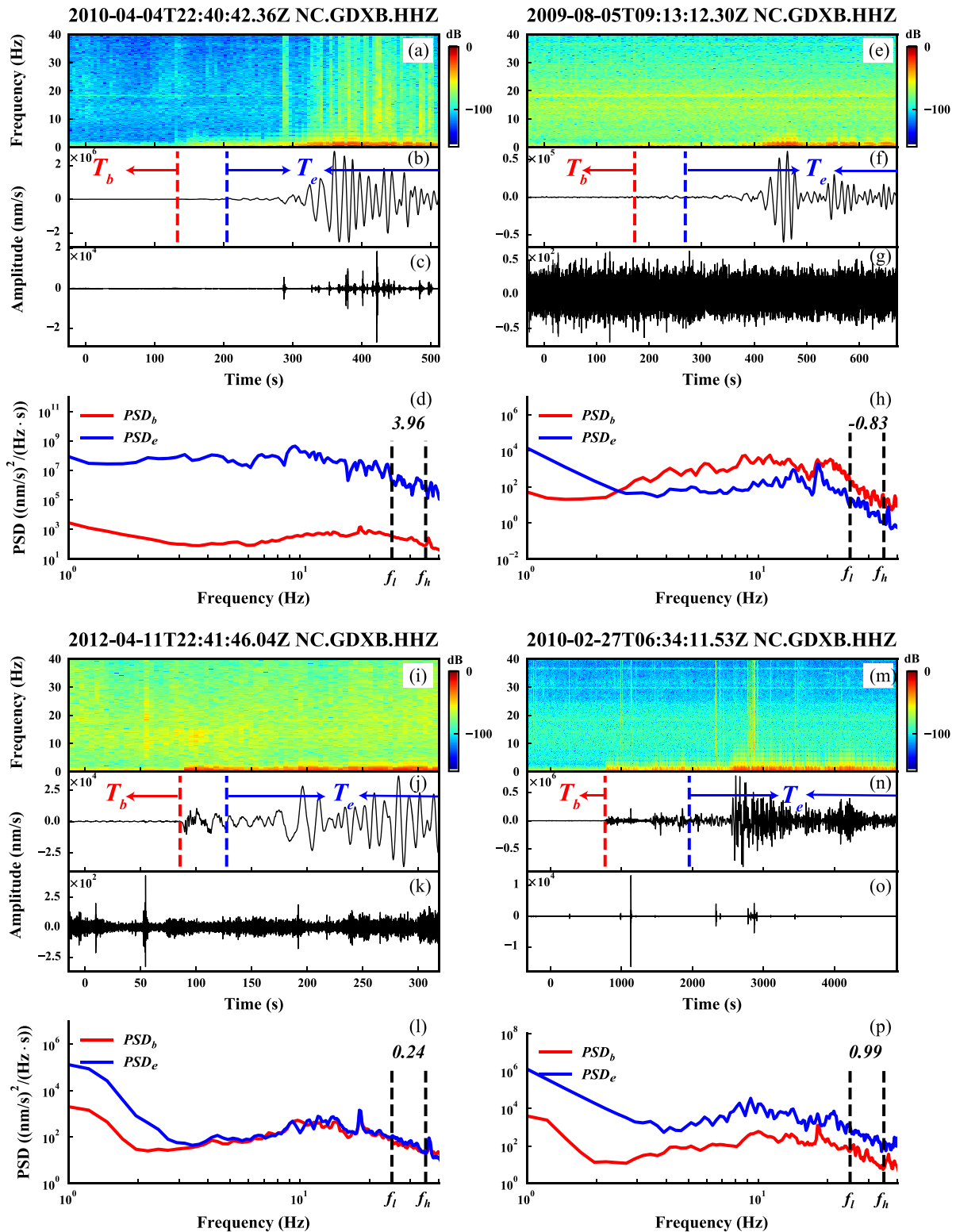


**Figure 1.** Dynamic triggering detection for the 4 April 2010  $M7.2$  Baja California (a–d), 5 August 2009  $M5.8$  Gulf of California (e–h), 11 April 2012  $M6$  Oregon coast (i–l), and 27 February 2010  $M8.8$  Chile earthquakes (m–p). (a–c) Spectrogram of the raw data, raw broadband seismogram, and high-pass-filtered ( $>25$  Hz) waveform recorded at Station GDXB in the Geysers area for the 2010 Baja California earthquake. The red and blue dashed lines mark the arrival times of  $P$  wave and a wave with the speed of  $5$  km/s.  $T_b$  represents the 5-hr time window before the  $P$  arrival, and  $T_e$  represents the time window between the arrival times of waves with speeds of  $5$  and  $2$  km/s. (d) Power spectral density (PSD) of the raw seismic data within  $T_b$  ( $PSD_b$ ) and  $T_e$  ( $PSD_e$ ). The black dashed lines mark the lower ( $f_l$ ) and upper ( $f_h$ ) frequency limits for integrating the PSDs. The number in the top-right corner is the logarithmic ratio of the distant earthquake ( $R_E$ ).

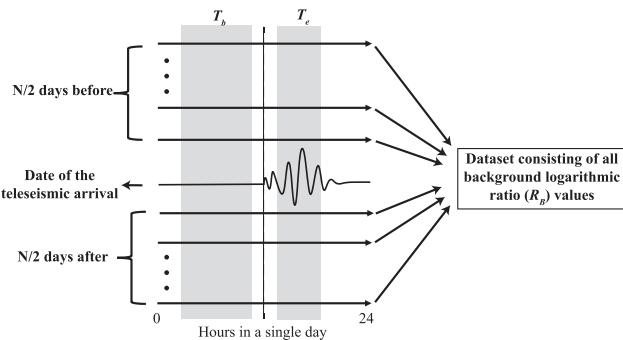


**Figure 2.** A schematic diagram for calculating the data set of background logarithmic ratio ( $R_B$ ).

## 2.2. Statistics on the Background High-Frequency Energy Variation

Although an  $R_E$  value larger than zero may be indicative of dynamic triggering, we still have to overcome two critical challenges. First, we need to consider the variation in noise levels. High-frequency noise during teleseismic waves may result in positive  $R_E$  values and thus cause false detections. For instance, no local earthquakes during the distant waves from the 11 April 2012 M6 Oregon coast earthquake are visible in both the spectrogram (Figure 1i) and high-pass-filtered ( $>25$  Hz) waveform (Figure 1k). However, the  $R_E$  value is 0.24 owing to the noise within the  $T_e$  time window, making it unreliable to rely on just the  $R_E$  value to identify dynamic triggering as shown in Figure 1l. Conversely, the high-frequency noise energy in  $T_b$  may lead to a low  $R_E$  value, even when there are triggered local earthquakes.

Second, a large  $R_E$  value itself may not always point to dynamic triggering, unless we verify that local earthquakes during the teleseismic wave train are not coincidences. For example, there are local events before the teleseismic arrival of the 27 February 2010 M8.8 Chile earthquake (Figure 1o). Although there are also local earthquakes during the surface waves, we need to determine whether they are triggered or merely background seismicity.

The key to tackling the two challenges is to estimate the variation in high-frequency energy between  $T_b$  and  $T_e$  in background days without the impact of distant earthquakes, which includes changes in both noise and background seismicity. As shown in Figure 2, for each distant earthquake, we select a total of  $N$  days before and after the date of the teleseismic arrival to represent the background. Then, we calculate the logarithmic ratio for each background day ( $R_B$ ) using the same  $T_b$  and  $T_e$  as those on the date of the distant earthquake based on equation (3). The data set consisting of the  $R_B$  values for all background days will then represent the variation in the background high-frequency energy. Taking consistent  $T_b$  and  $T_e$  windows for background days and distant earthquake can avoid the impact on  $R_B$  of temporal variations of noise and background seismicity in a day. To ensure a statistical significance, the number of background days  $N$  need to be sufficiently large. In addition, to avoid including local events triggered by other distant earthquakes in the background days, we remove outliers in the data set of  $R_B$ , which are defined by differing from the mean by more than 3 times the variance.

Figure 3 shows the data sets of  $R_B$  values obtained for the four teleseismic earthquakes in Figure 1 with  $N = 120$ . The histogram shows the probability density of  $R_B$  values. All the four mean values are negative, indicating variations in the background high-frequency energy; thus, we have to compare the logarithmic ratios of the distant earthquakes  $R_E$  and the mean  $R_B$  value to reflect dynamic triggering. The  $R_E$  value of the 2010 Baja California earthquake is well above the mean  $R_B$  value (Figure 3a; triggering); while the  $R_E$  value is close to the mean  $R_B$  for the 2009 Gulf of California earthquake (Figure 3b; no triggering). However, the  $R_E$  values of the 2012 Oregon coast and 2010 Chile earthquakes are not significantly larger than the respective mean values of  $R_B$  (Figures 3c and 3d), indicating that it is still difficult to tell whether there are dynamic triggering or not.

## 2.3. Confidence Level of Dynamic Triggering

To quantify the significance of dynamic triggering, we should not only use the mean value but also take into account the deviation of the  $R_B$  data set. As shown in Figure 3, we fit the histogram of the  $R_B$  data set for each distant earthquake with a normal distribution (see supporting information) to obtain a probability density function (PDF).

Furthermore, we define the confidence level ( $CL$ ; Daley & Vere-Jones, 2003) of the dynamic triggering by calculating the probability for  $R_B \leq R_E$ :

$$CL(R_E) = \int_{-\infty}^{R_E} PDF \, dR_B. \quad (4)$$

By definition, the confidence level is the area under the PDF curve from minus infinity to  $R_E$ , ranging from zero to one. If the whole PDF curve is on the left side of a certain  $R_E$  (i.e.,  $R_E \gg \mu + 2\sigma$ , where  $\mu$  and  $\sigma$  are the

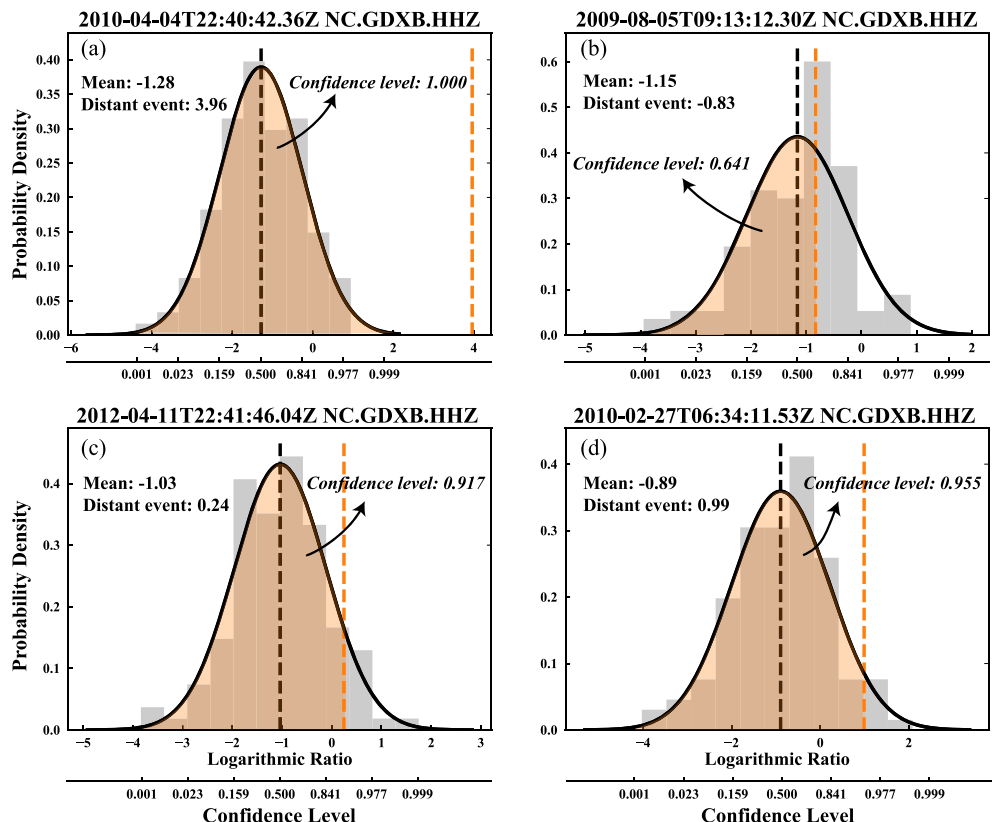


**Figure 3.** Statistics of  $R_B$  data set (with  $N = 120$ ) for the four teleseismic earthquakes shown in Figure 1. In each panel, the histogram shows the probability density of  $R_B$  values. The height of each gray bar is the number of the background days within the  $R_B$  bin normalized by the total number of the background days and the width of the bin. The black solid line is the probability density function (PDF) acquired by fitting the data set to a normal distribution with the mean indicated by the black dashed line. The orange dashed line marks the  $R_E$  value for the distant earthquake. The mean of the PDF and  $R_E$  value are given in the upper left in each panel. The orange shaded area enclosed by the PDF curve and the orange dashed line is the confidence level of dynamic triggering, which is shown on the bottom axis corresponding to different  $R_E$  values.

mean and standard deviation of the normal distribution, respectively), the confidence level will then be 1.000 (Figure S2). For a normal distribution,

$$\int_{-\infty}^{\mu+2\sigma} \text{PDF } dR_B \approx 0.977. \quad (5)$$

Thus, the confidence level corresponding to  $2\sigma$  (i.e.,  $R_E = \mu + 2\sigma$ ) is 0.977, marking a high threshold to determine dynamic triggering. We may lower the level to  $\sigma$ , yielding a confidence value of 0.841, which may serve as a lower threshold to clearly identify triggering.

We then calculate the confidence levels of the four teleseismic earthquakes in Figure 3. The confidence level for the 2010 Baja California is 1.000, indicating triggering with 100% confidence. In contrast, the 2009 Gulf of California earthquake has a very low confidence level of triggering (0.641). For the 2012 Oregon coast and 2010 Chile earthquakes, we obtain confidence levels of 0.917 and 0.955 ( $\sigma < R_E - \mu < 2\sigma$ ), respectively, indicating possible triggerings with moderate confidence levels.

### 3. Application of the HiFi Method to the Geysers Geothermal Field

#### 3.1. Study Area and Data

The Geysers Geothermal Field in California is a notable geothermal/volcanic region with active faults and obvious fluid motions leading to high background seismicity and susceptibility to dynamic triggering (Brodky, 2006; Gomberg et al., 2001; Gomberg & Davis, 1996; Prejean et al., 2004; Stark & Davis, 1996).

Aiken and Peng (2014) systematically investigated the reaction of the Geysers area to distant earthquakes from 2000 to 2012 by identifying local earthquakes manually and estimating the seismicity change using the  $\beta$  statistic test. Here we investigate the dynamic triggering for the distant earthquakes occurred during the same time span using the HiFi method.

We chose the distant earthquakes from the Advanced National Seismic System (U.S. Geological Survey, 2017) catalog based on the depths, magnitudes, and epicentral distances according to Aiken and Peng (2014). The selected events have focal depths of less than 100 km that produce strong surface waves. Moreover, two groups of distant earthquakes were chosen with different magnitudes and distances from Station GDX/GDXB (Figure S1). In May 2006, short-period instruments at Station GDX were upgraded to broadband sensors, and the station was renamed GDXB. The first group consists of earthquakes with magnitudes of 5.5–7.5 and epicentral distances of 100–2,000 km; and the second group comprises events with magnitudes  $\geq 7.5$  and epicentral distances larger than 2,000 km. The distance ensures that transient dynamic stresses dominate the static stress (Freed, 2005; King et al., 1994), while the magnitude assures sufficient dynamic stresses for triggering. Continuous seismic records at Station GDX/GDXB are downloaded from the Northern California Earthquake Data Center (NCEDC, 2014) and are used to detect high-frequency energy variation. The final data set contains 112 distant earthquakes with complete records from 5 hr before the teleseismic arrivals, including the above four examples discussed in section 2. Event information as well as their dynamic triggering analyses are listed in Table S1.

### 3.2. Parameter Setting for the HiFi Method

We use the same  $T_b$  and  $T_e$  windows as in Aiken and Peng (2014) so as to directly compare the two sets of results.  $T_b$  is 5 hr before the  $P$  wave arrival of the distant earthquake, and  $T_e$  is between arrivals of two teleseismic waves with speeds of 5 and 2 km/s. For the number of background days  $N$ , we have tested six different values including 60, 120, 180, 240, 300, and 360.

The lower limit  $f_l$  depends on the epicentral distances of distant earthquakes. For events that are very far away,  $f_l = 5$  Hz could avoid most of teleseismic signals. Taking the 1 April 2007  $M8.1$  Solomon Islands earthquake as an example (Figures S3a–S3c; without triggered earthquakes), we test the frequency ranges of 5–35, 10–35, 15–35, 20–35, and 25–35 Hz. The confidence levels are small, and their variations are not significant (Figure S3d). In contrast, several distant earthquakes are close ( $<500$  km) to the Geysers area, so that their body-wave energies are still rich at  $\sim 20$  Hz. For the 17 June 2005  $M6.6$  Northern California earthquake (Figures S3e–S3g; without triggered earthquakes), the confidence levels are very large when  $f_l < 15$  Hz due to the energies of teleseismic waves (Figure S3h) and thus may lead to false detection of dynamic triggering. The variations in confidence levels of all distant earthquakes are shown in Figure S4 and listed in Table S2. Most of them are small, indicating little effect of frequency ranges. Therefore, we chose the frequency range of 25–35 Hz for all events. To verify that this frequency range can contain the energies of local earthquakes, we further examine the energy distribution of local events in the Northern California Earthquake Catalog from the Northern California Earthquake Data Center (NCEDC, 2014). Local event energies are significantly larger than the background ones at 25–35 Hz (Figure S5).

### 3.3. Results

The mean values and standard deviations of confidence levels for different  $N$  values are calculated for all distant earthquakes (Table S1). The standard deviations are generally small (Figure 4a), suggesting that the impact of different  $N$  on the confidence level is not significant. The mean confidence levels of 93 distant events are smaller than 0.841 (i.e.,  $R_E - \mu < \sigma$ ), which are thus considered not to have caused any remote triggering. There are nine distant earthquakes with mean confidence levels between  $\sigma$  and  $2\sigma$ . Ten out of the 112 distant events have mean confidence levels larger than the 0.977, that is,  $R_E - \mu > 2\sigma$  (Figure 4), likely to trigger local earthquakes.

To confirm whether the 10 distant events triggered local earthquakes or not, we visually inspect their spectrograms and waveforms recorded at GDX/GDXB and neighboring stations (Figure S1). Local earthquakes are identified by waveforms recorded at more than two stations. Based on this criterion, we confirm local events during the wave trains from eight distant earthquakes (Table S1 and Figures S5–S8). The remaining two events are the 22 December 2003  $M6.5$  Central California and 30 July 2006  $M5.9$  Gulf of California earthquakes with mean confidence levels of 1.000 and 0.996, respectively. There are high-frequency signals

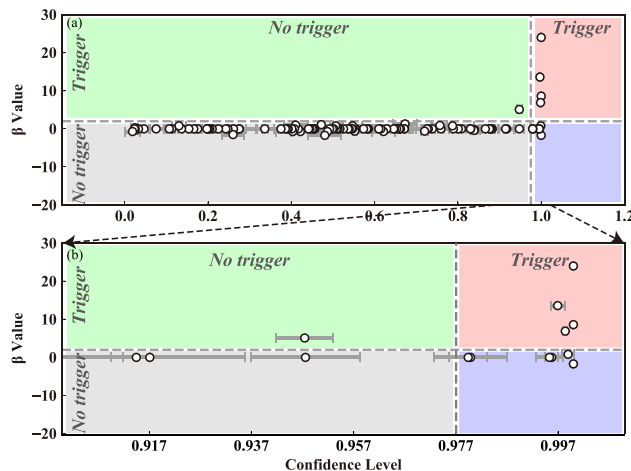


**Figure 4.** Results of dynamic triggering determinations by the High-Frequency power Integral ratio (HiFi) method and  $\beta$  statistic in the Geysers region (Aiken & Peng, 2014). (a) Circles and gray error bars mark the means and standard deviations of the confidence levels for different  $N$  values. The horizontal and vertical dashed lines mark the  $\beta$  value threshold 2 and the confidence-level threshold 0.977, respectively. The red, green, and blue areas represent regions of  $\beta$  value and confidence level where teleseismic events are determined as triggering by both the HiFi method and  $\beta$  statistic, by the  $\beta$  statistic only, and by the HiFi method only, respectively (TT, TF, and FT in short). The gray area encloses events without triggering by both methods (FF in short). (b) A zoom-in plot in the vicinity of the confidence-level threshold.

during their waves at Station GDX/GDXB but are likely noises because we cannot find corresponding local seismic waveforms at other nearby stations (Figures S9 and S10). Therefore, applications of the HiFi method at multiple stations could suppress such noise effect and thus avoid false detections in future work.

## 4. Discussion

### 4.1. Comparison With $\beta$ Statistic

We compare our results with those obtained using the  $\beta$  statistic (Aiken & Peng, 2014). The  $\beta$  values are calculated when at least one microearthquake is identified during the teleseismic wave train (Table S1). Otherwise, it is set to zero. The values of confidence levels and  $\beta$  for most of the events are positively correlated (Figure 4). As stated in section 2.3, a safe  $2\sigma$  confidence-level threshold for dynamic triggering is 0.977. In the meantime, a widely used threshold for the  $\beta$  value is 2.0 (Reasenberg & Simpson, 1992). Using the two thresholds, we divide the distant events into four groups (Figure 4). Four earthquakes have passed the thresholds of both the  $\beta$  statistic and HiFi method and thus are confirmed as dynamic triggering (TT in short). Together with the events that have failed to pass the thresholds of both the  $\beta$  statistic and our HiFi method (FF in short), 94% of the examined distant events have the same triggering results by the two methods.

However, six events exceed the HiFi confidence-level threshold but fail in  $\beta$  statistic (FT in short). As discussed in section 3.3, four out of the six events did have triggered local earthquakes recorded by at least five stations during the passage of their waves (Figures S5–S8). The difference in the significance evaluation using  $\beta$  value and confidence level is due

to the fact that the  $\beta$  value is dependent on the completeness of local earthquakes, while our confidence level is independent of the number of local events, as we compare the high-frequency energy variation. Moreover, the 27 February 2010 M8.8 Chile earthquake only passes the  $\beta$  statistic test, but its confidence level is lower than the  $2\sigma$  requirement (TF in short). Local earthquakes are found in both  $T_b$  and  $T_e$  (Figures 1m and 1o). There are more local events in  $T_e$  than in  $T_b$ , resulting in a  $\beta$  value of 5.1. In the HiFi method, the mean confidence level is also quite high (0.947), slightly less than the  $2\sigma$  threshold (0.977). If we lower the threshold, the 2010 Maule earthquake would satisfy the requirement, raising the question of how to define a more effective threshold of the confidence level.

### 4.2. Optimal Confidence-Level Threshold

If we have sufficiently large amounts of data, we may be able to determine the perfect threshold of the confidence level by finding the boundary separating triggering and nontriggering. However, in reality, we have to find an optimal threshold given the limited number of large earthquakes that dynamically triggered local earthquakes and discrete confidence levels in the Geysers area.

We use the receiver operating characteristics method (e.g., Fawcett, 2006; Metz, 1978) to estimate the similarity between the triggering results of the HiFi method and  $\beta$  statistic (Aiken & Peng, 2014) at different confidence-level thresholds (see supporting information). The similarity is measured by the true positive rate (TPR) and false positive rate (FPR), representing the rate of same and different triggering results between the two methods, respectively:

$$\text{TPR} = \frac{N_{\text{TT}}}{N_{\text{TT}} + N_{\text{TF}}}, \quad (6)$$

$$\text{FPR} = \frac{N_{\text{FT}}}{N_{\text{FT}} + N_{\text{FF}}}. \quad (7)$$

TPR and FPR are calculated by the number of distant earthquakes in the four groups defined in Figure 4 ( $N_{\text{TF}}$ ,  $N_{\text{TT}}$ ,  $N_{\text{FF}}$ , and  $N_{\text{FT}}$ ). If we regard all the triggering results based on  $\beta$  statistic as true, the triggering

results of the HiFi method should be most consistent with the truth at the optimal threshold. Therefore, the optimal threshold corresponds to the largest value of TPR minus FPR. From our result, the range of optimal threshold values is determined to be 0.918–0.947 for the Geysers area (Figure S12). With the locally determined optimal threshold ranges, the HiFi method can be applied to other distant earthquakes to achieve automated and reliable detection of dynamic triggering. In addition, more results of dynamic triggering can provide further constraints for better determinations of optimal threshold by the receiver operating characteristics method.

## 5. Conclusions

In this study, we develop a new method for automatic detection of dynamic triggering based on the HiFi. The HiFi method differs from the traditional methods in two aspects. First, it does not rely on the number of local earthquakes by directly integrating the high-frequency energy to represent the level of local seismicity. Second, the HiFi method takes into account variations in the background seismicity and suppresses the noise effect by statistics. Such characteristics enable automated detection of dynamic triggering and thus can process large amounts of data to systematically investigate dynamic triggering so as to better understand stress variations in earthquake prone areas.

We applied the HiFi method to analyze 112 teleseismic earthquakes recorded in the Geysers area. Ten out of the 112 events have quite high confidence levels larger than 0.977 ( $2\sigma$ ), although only eight are confirmed to have triggered local earthquakes after visual inspections. Ninety-four percent of our results are the same with those of  $\beta$  statistic, and we suggest that the optimal threshold range for the Geysers area to be 0.918–0.947.

## Acknowledgments

Waveform data and local earthquake catalog for this study are obtained at the Northern California Earthquake Data Center (NCEDC; doi:10.7932/NCEDC). The distant earthquake catalog is from the Advanced National Seismic System (ANSS; doi: 10.5066/F7MS3QZH). We are very grateful to those agencies for sharing their data. We are grateful to Prof. Jiancang Zhuang and Prof. Zhigang Peng for their thoughtful advice. We thank the reviewers and editor for their insightful comments. This work is jointly supported by the National Key R&D Program of China (Grant 2018YFC1503401), the National Nature Science Foundation of China project (Grant 41674047), the Hong Kong Research Grant Council (Grant 14305617), and China Earthquake Science Experiment Project, CEA (Grant 2019CSES0107).

## References

- Aiken, C., & Peng, Z. (2014). Dynamic triggering of microearthquakes in three geothermal/volcanic regions of California. *Journal of Geophysical Research: Solid Earth*, 119, 6992–7009. <https://doi.org/10.1002/2014JB011218>
- Anderson, J. G., Brune, J. N., Louie, J. N., Zeng, Y., Savage, M., Yu, G., et al. (1994). Seismicity in the western Great Basin apparently triggered by the Landers, California, earthquake, 28 June 1992. *Bulletin of the Seismological Society of America*, 84(3), 863–891.
- Brodsky, E. E. (2006). Long-range triggered earthquakes that continue after the wave train passes. *Geophysical Research Letters*, 33, L15313. <https://doi.org/10.1029/2006GL026605>
- Brodsky, E. E., & Prejean, S. G. (2005). New constraints on mechanisms of remotely triggered seismicity at Long Valley Caldera. *Journal of Geophysical Research*, 110, B04302. <https://doi.org/10.1029/2004JB003211>
- Brodsky, E. E., & van der Elst, N. J. (2014). The uses of dynamic earthquake triggering. *Annual Review of Earth and Planetary Sciences*, 42(1), 317–339. <https://doi.org/10.1146/annurev-earth-060313-054648>
- Cochran, E. S., Vidale, J. E., & Tanaka, S. (2004). Earth tides can trigger shallow thrust fault earthquakes. *Science*, 306(5699), 1164–1166. <https://doi.org/10.1126/science.1103961>
- Daley, D. J., & Vere-Jones, D. (2003). *An introduction to the theory of point processes*, (2nd ed., Vol. 1, p. 469). New York: Springer. <https://doi.org/10.1007/b97277>
- Fawcett, T. (2006). An introduction to ROC analysis. *Pattern Recognition Letters*, 27(8), 861–874. <https://doi.org/10.1016/j.patrec.2005.10.010>
- Freed, A. M. (2005). Earthquake triggering by static, dynamic, and postseismic stress transfer. *Annual Review of Earth and Planetary Sciences*, 33(1), 335–367. <https://doi.org/10.1146/annurev.earth.33.092203.122505>
- Gibbons, S. J., & Ringdal, F. (2006). The detection of low magnitude seismic events using array-based waveform correlation. *Geophysical Journal International*, 165(1), 149–166. <https://doi.org/10.31223/osf.io/5z9ew>
- Gomberg, J., Bodin, P., Larson, K., & Dragert, H. (2004). Earthquake nucleation by transient deformations caused by the  $M = 7.9$  Denali, Alaska, earthquake. *Nature*, 427, 621–624. <https://doi.org/10.1038/nature02335>
- Gomberg, J., & Davis, S. (1996). Stress/strain changes and triggered seismicity at The Geysers, California. *Journal of Geophysical Research*, 101(B1), 733–749. <https://doi.org/10.1029/95JB03250>
- Gomberg, J., & Johnson, P. (2005). Dynamic triggering of earthquakes. *Nature*, 437(7060), 830. <https://doi.org/10.1038/437830a>
- Gomberg, J., Reasenberg, P., Bodin, P. I., & Harris, R. (2001). Earthquake triggering by seismic waves following the Landers and Hector Mine earthquakes. *Nature*, 411(6836), 462–466. <https://doi.org/10.1038/35078053>
- Hill, D. P., & Prejean, S. (2007). Dynamic triggering. In H. Kanamori, & G. Schubert (Eds.), *Treatise on geophysics*, (Vol. 4, pp. 257–292). Amsterdam, Netherlands: Elsevier. <https://doi.org/10.1016/b978-044452748-6.00070-5>
- Hill, D. P., Reasenberg, P. A., Michael, A., Arabaz, W. J., Beroza, G., Brumbaugh, D., et al. (1993). Seismicity remotely triggered by the magnitude 7.3 Landers, California, earthquake. *Science*, 260(5114), 1617–1623. <https://doi.org/10.1126/science.260.5114.1617>
- Jiang, T., Peng, Z., Wang, W., & Chen, Q. F. (2010). Remotely Triggered Seismicity in Continental China following the 2008 Mw 7.9 Wenchuan Earthquake. *Bulletin of the Seismological Society of America*, 100(5B), 2574–2589. <https://doi.org/10.1785/0120090286>
- Johnston, M., Prejean, S., & Hill, D. (2004). Triggered deformation and seismic activity under Mammoth Mountain in long Valley caldera by the 3 November 2002  $M_w$  7.9 Denali fault earthquake. *Bulletin of the Seismological Society of America*, 94(6B), S360–S369. <https://doi.org/10.1785/0120040603>
- King, G. C., Stein, R. S., & Lin, J. (1994). Static stress changes and the triggering of earthquakes. *Bulletin of the Seismological Society of America*, 84(3), 935–953.

- Linville, L., Pankow, K., Kilb, D., & Velasco, A. (2014). Exploring remote earthquake triggering potential across EarthScopes' Transportable Array through frequency domain array visualization. *Journal of Geophysical Research: Solid Earth*, 119, 8950–8963. <https://doi.org/10.1002/2014JB011529>
- Matthews, M. V., & Reasenberg, P. A. (1988). Statistical methods for investigating quiescence and other temporal seismicity patterns. *Pure and Applied Geophysics*, 126(2-4), 357–372. <https://doi.org/10.1007/bf00879003>
- Metz, C. E. (1978). Basic principles of ROC analysis. *Seminars in Nuclear Medicine*, 8(4), 283–298. [https://doi.org/10.1016/s0001-2998\(78\)80014-2](https://doi.org/10.1016/s0001-2998(78)80014-2)
- Miyazawa, M., & Mori, J. (2005). Detection of triggered deep low-frequency events from the 2003 Tokachi-oki earthquake. *Geophysical Research Letters*, 32, L10307. <https://doi.org/10.1029/2005GL022539>
- NCECD (2014). Northern California Earthquake Data Center. UC Berkeley Seismological Laboratory. Dataset. <https://doi.org/10.7932/NCECD>.
- Pankow, K. L., Arabasz, W. J., Pechmann, J. C., & Nava, S. J. (2004). Triggered seismicity in Utah from the 3 November 2002 Denali Fault Earthquake. *Bulletin of the Seismological Society of America*, 94(6B), S332–S347. <https://doi.org/10.1785/0120040609>
- Peng, Y., Zhou, S., Zhuang, J., & Shi, J. (2012). An approach to detect the abnormal seismicity increase in Southwestern China triggered coseismically by 2004 Sumatra  $M_w$  9.2 earthquake. *Geophysical Journal International*, 189(3), 1734–1740. <https://doi.org/10.1111/j.1365-246x.2012.05456.x>
- Peng, Z., Vidale, J. E., Wech, A. G., Nadeau, R. M., & Creager, K. C. (2009). Remote triggering of tremor along the San Andreas Fault in central California. *Journal of Geophysical Research*, 114, B00A06. <https://doi.org/10.1029/2008JB006049>
- Peng, Z., Wang, W., Chen, Q. F., & Jiang, T. (2010). Remotely triggered seismicity in north China following the 2008  $M_w$  7.9 Wenchuan earthquake. *Earth, Planets and Space*, 62(11), 893–898. <https://doi.org/10.5047/eps.2009.03.006>
- Peng, Z., & Zhao, P. (2009). Migration of early aftershocks following the 2004 Parkfield earthquake. *Nature Geoscience*, 2(12), 877–881. <https://doi.org/10.1038/ngeo697>
- Prejean, S. G., Hill, D. P., Brodsky, E. E., Hough, S. E., Johnston, M. J. S., Malone, S. D., et al. (2004). Remotely triggered seismicity on the United States west coast following the  $M_w$  7.9 Denali fault earthquake. *Bulletin of the Seismological Society of America*, 94(6B), S348–S359. <https://doi.org/10.1785/0120040610>
- Reasenberg, P. A., & Simpson, R. W. (1992). Response of regional seismicity to the static stress change produced by the Loma Prieta earthquake. *Science*, 255(5052), 1687–1690. <https://doi.org/10.1126/science.255.5052.1687>
- Stark, M. A., & Davis, S. D. (1996). Remotely triggered microearthquakes at the Geysers Geothermal Field, California. *Geophysical Research Letters*, 23(9), 945–948. <https://doi.org/10.1029/96GL00011>
- U.S. Geological Survey, Earthquake Hazards Program (2017). Advanced National Seismic System (ANSS) Comprehensive Catalog of Earthquake Events and Products: Various, <https://doi.org/10.5066/F7MS3QZH>.
- Van der Elst, N. J., Savage, H. M., Keranen, K. M., & Abers, G. A. (2013). Enhanced remote earthquake triggering at fluid-injection sites in the midwestern United States. *Science*, 341(6142), 164–167. <https://doi.org/10.1126/science.1238948>
- Velasco, A. A., Alfaro-Diaz, R., Kilb, D., & Pankow, K. L. (2016). A time-domain detection approach to identify small earthquakes within the continental United States recorded by the USArray and regional networks. *Bulletin of the Seismological Society of America*, 106(2), 512–525. <https://doi.org/10.1785/0120150156>
- Velasco, A. A., Hernandez, S., Parsons, T., & Pankow, K. (2008). Global ubiquity of dynamic earthquake triggering. *Nature Geoscience*, 1(6), 375–379. <https://doi.org/10.1038/ngeo204>
- Wang, B., Harrington, R. M., Liu, Y., Yu, H., Carey, A., & Elst, N. J. (2015). Isolated cases of remote dynamic triggering in Canada detected using catalogued earthquakes combined with a matched-filter approach. *Geophysical Research Letters*, 42, 5187–5196. <https://doi.org/10.1002/2015GL064377>
- Wu, C., Peng, Z., Wang, W., & Chen, Q. F. (2011). Dynamic triggering of shallow earthquakes near Beijing, China. *Geophysical Journal International*, 185(3), 1321–1334. <https://doi.org/10.1111/j.1365-246x.2011.05002.x>
- Yang, H., Zhu, L., & Chu, R. (2009). Fault-plane determination of the 18 April 2008 Mount Carmel, Illinois, Earthquake by detecting and relocating aftershocks. *Bulletin of the Seismological Society of America*, 99(6), 3413–3420. <https://doi.org/10.1785/0120090038>